applied nano

MDPI

Article

Influence of the Parameters of Cluster Ions on the Formation of Nanostructures on the KTP Surface

Ivan V. Nikolaev * and Nikolay G. Korobeishchikov

Department of Applied Physics, Novosibirsk State University, Pirogov Str. 2, 630090 Novosibirsk, Russia; korobei@ci.nsu.ru

* Correspondence: i.nikolaev@nsu.ru

Abstract: In this work, the formation of periodic nanostructures on the surface of potassium titanyl phosphate (KTP) has been demonstrated. The surface of KTP single crystals after the processing of argon cluster ions with different energy per cluster atom E/N_{mean} = 12.5 and 110 eV/atom has been studied using atomic force microscopy (AFM). To characterize the nanostructures, the power spectral density (PSD) functions have been used. The features of the formation of periodic nanostructures are revealed depending on the incident angle of clusters and different energy per atom in clusters.

Keywords: cluster ion beam; nanostructures; potassium titanyl phosphate; atomic force microscopy; power spectral density function

Citation: Nikolaev, I.V.; Korobeishchikov, N.G. Influence of the Parameters of Cluster Ions on the Formation of Nanostructures on the KTP Surface. *Appl. Nano* **2021**, *2*, 25–30. https://doi.org/10.3390/applnanao20100003

Received: 27 November 2020
Accepted: 8 January 2021
Published: 23 January 2021

1. Introduction

Potassium titanyl phosphate ($KTiOPO_4$, KTP) is one of the well-known nonlinear optical materials and widely used in devices for parametric generation, high-power lasers, and electro-optical modulators with high efficiency of frequency conversion, optical waveguides in integrated optics, etc. [1,2].

It was previously shown that the monomer ion beam can form self-organized periodic nanostructures on the surface of various materials [3–6]. Such structures on surfaces attract interest for wide practical use [7]. Although gas cluster ion beams (GCIB) is commonly used for highly efficient surface smoothing, it can also be used to form nanostructures [8–12]. It should be noted that cluster ions do less damage to the subsurface layer after processing since they have a shallower impact depth and can be lower energies per atom compared to monomer ions [9–12]. As a rule, for the formation of nanostructures, cluster beams with low energies per atom in a cluster (about several eV) are used [8–11]. This work compares the efficiency of the formation of nanostructures by gas clusters with low and high energy per atom in the cluster.

2. Materials and Methods

KTP single crystals were preliminarily polished by the chemical-mechanical method. As-prepared samples are commercial single crystals of potassium titanyl phosphate made by "Siberian Monocrystal–EKSMA" Company (Novosibirsk, Russia). The KTP surface treatment by cluster ions was performed in an experimental setup described in Ref. [12]. The cluster beam was formed by adiabatic expansion of high purity argon [13]. The cluster ion beam parameters were determined using the time-of-flight technique [14]. To study the influence of the parameters of cluster ions on the processing of the KTP surface, significantly different energies per atom in cluster E/N_{mean} were selected: 12.5 eV/atom (low-energy mode) and 110 eV/atom (high-energy mode). The kinetic cluster energy E was 10 and 22 keV with the average cluster size N_{mean} = 800 and 200 atoms/cluster, respectively. In addition, we varied the incident angles of the cluster-ion beam from 0° to 70° (from the surface normal). For the correct comparison of surfaces after processing, we used the same sample.

The target surfaces were characterized using atomic force microscopy (AFM, NTegra Prima HD). The scan size of AFM measurements was 2 × 2 μm^2 with a resolution of 1024 × 1024 pixels. Additionally, we analyzed the power spectral density (PSD) functions before and after processing. The PSD function is the Fourier transform of the distribution of irregularity heights on the surface, and it is the function depending on spatial frequency ν [15–17]. We clarify here that the spatial frequency ν is a measure of how often the same height repeats per unit of distance [14]. The PSD function is helpful to determine the effective roughness σ_{eff} [12], which takes into account the lateral roughness as opposed to the convention root–mean–square (RMS) roughness R_q.

The effective roughness σ_{eff} and the PSD function are related as follows:

$$\sigma_{eff}^2 = 2\pi \int_{\nu_{min}}^{\nu_{max}} PSD_{2D}(\nu) d\nu, \quad (1)$$

where $\nu_{min} = 1/L$ and $\nu_{max} = 1/\Delta x$, L—linear size of the scan area, and Δx—distance between adjacent measured points.

3. Results and Discussion

3.1. Formation of Nanostructures on the Surface of KTP Single Crystals

The maximum ion fluencies were 2 × 10^{16} ions/cm^2 in the low-energy mode (Figure 1) and 3 × 10^{15} ions/cm^2 in the high-energy mode (Figure 2). Despite the fact that the ion fluence in the high-energy mode was an order of magnitude lower, we assume that it is more correct to compare at the same etching depths because the formed nanostructures are nothing more than displaced surface material [8–11]. An aperture mask was used to estimate the etching depth and to obtain many processed areas (with different angles of incidence) on one sample. After processing, a step was formed at the "processed region–unprocessed region" boundary, the height of which was measured by AFM. The average etching depth $\langle H_{etching} \rangle$ was estimated from measurements in 9 areas of the formed step. The average etching depths were close—$\langle H_{etching} \rangle_1$ = 40 nm for low-energy mode and $\langle H_{etching} \rangle_2$ = 55 nm for high-energy mode.

Figure 1 shows 2D images and profiles of the KTP surface as-prepared and after processing by argon cluster ions at the low-energy mode (E/N_{mean} = 12.5 eV/atom) at the different incident angles. The lowest point of the profile corresponds to Z = 0 nm. A slight change in the surface profile is observed after treatment at the incident angles less than 45°, and the maximum height R_t decreases from 2.5 to 2 nm. At larger incident angles (≥45°), the maximum height R_t increases significantly (by 16–24 times compared to the original surface) due to the formation of periodic nanostructures. As can be seen in Figure 1, the highest height of ripples is observed at the incident angle of 70° (Figure 1f) but the most ordered (including laterally) ripples—at 45° and 60° (Figure 1d,e). For clarity of differences in profiles both at different angles and for different treatment modes, the maximum height on the scale (in Figures 1 and 2) is selected according to the height of the highest surface profile (Figure 1f). As it is shown in Ref. [18], such nanostructures contribute to the quality improvement of the antireflective coatings.

Figure 2 shows 2D images and profiles of the KTP surface as-prepared and after processing by argon cluster ions at the high-energy mode (E/N_{mean} = 110 eV/atom). First, periodic nanostructures are not observed even at incident angles of 45° and 60° (Figure 2d,e). Second, the maximum height of ripples is 10 nm at 70° (Figure 2f)—by 3 times lower than in low-energy mode. At first glance, it would seem that the high-energy treatment mode has better formation of periodic nanostructures due to high cluster energy. As seen in Figure 2, this is not the case.

We assume that this is due to the significant difference in sputtering yields of the two treatment modes—by 36 times: 100 cluster ions with E/N_{mean} = 110 eV/atom sputter 72 target atoms and 100 cluster ions with E/N_{mean} = 12.5 eV/atom sputter only 2 target atoms. Thus, a large proportion of cluster energy at the low-energy mode is spent not only on

sputtering (low sputtering yield) but also on the active lateral displacement of subsurface target atoms, i.e., the formation of periodic nanostructures.

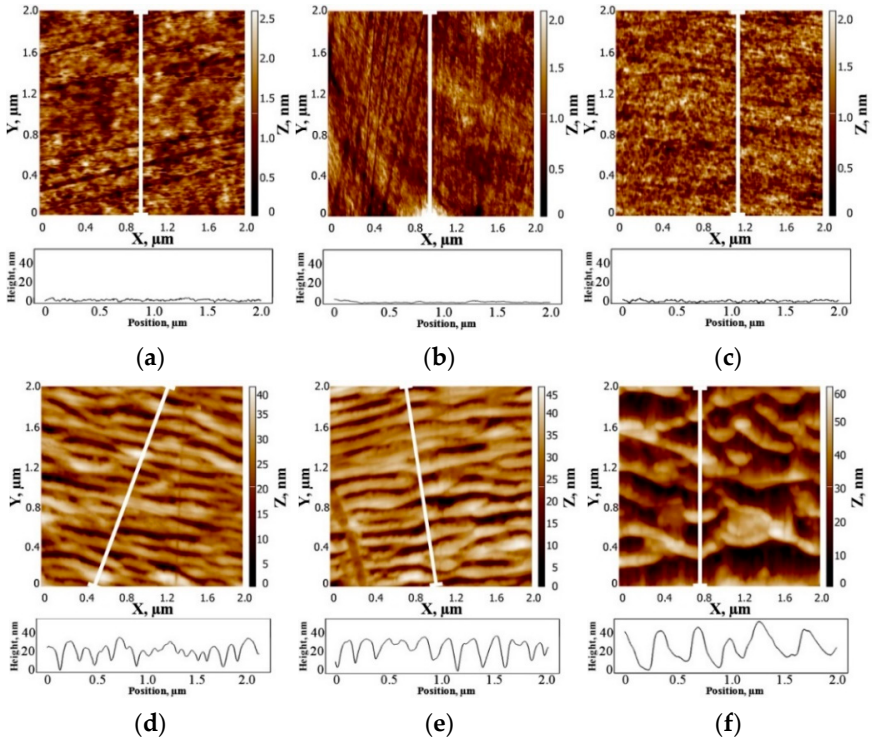

Figure 1. Atomic force microscopy (AFM) images and profiles of potassium titanyl phosphate (KTP) surface before (**a**) and after the low-energy treatment mode at different incident angles of cluster ions: (**b**) 0°, (**c**) 30°, (**d**) 45°, (**e**) 60°, and (**f**) 70°.

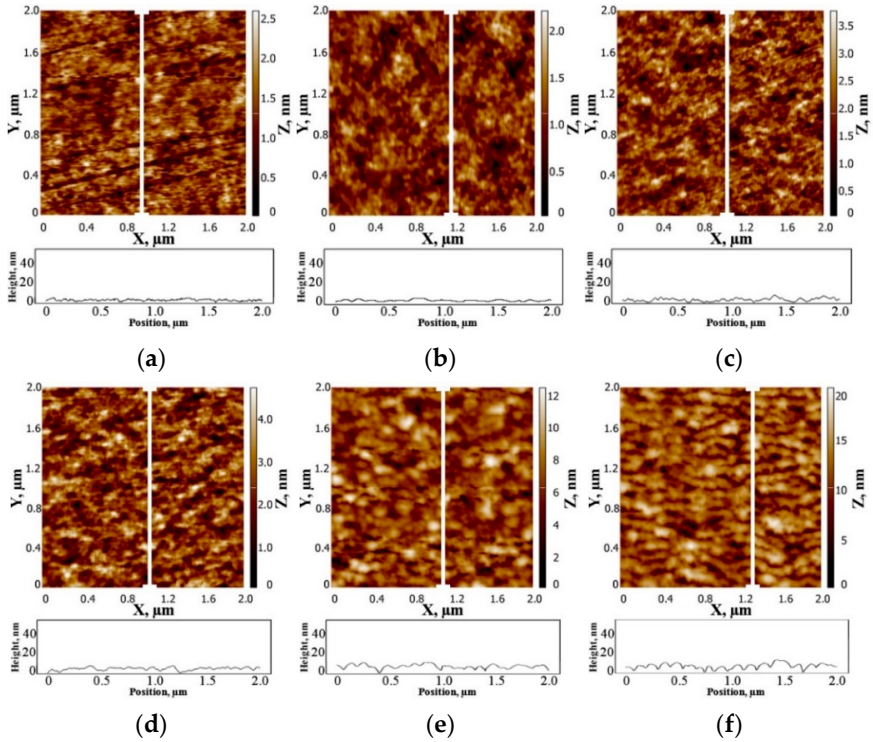

Figure 2. AFM images and profiles of KTP surface before (**a**) and after the high-energy treatment mode at different incident angles of cluster ions: (**b**) 0°, (**c**) 30°, (**d**) 45°, (**e**) 60°, and (**f**) 70°.

3.2. Power Spectral Density Functions

Figure 3 demonstrates the PSD functions of the KTP surface after processing at the different incident cluster angles for both treatment modes. In contrast to AFM images, PSD functions provide more quantitative data, especially for nanostructures. As can be seen in Figure 3a, low-energy mode smooths the KTP surface at small angles (≤30°) in the wide range of spatial frequencies ν from 1 to 8 μm^{-1} (30°) and to 15 μm^{-1} (0°). The self-organized nanostructures increase the surface roughness over the whole range of spatial frequencies. In Figure 3a, the pronounced peaks (marked by arrows) are observed. Each peak characterizes the frequency of self-organized nanostructures. It should be noted that the peak shift corresponds to the change of characteristic size (wavelength) of the nanostructure, which increases with increasing the incident angle, i.e., 167, 200, 334–500 nm for 45°, 60°, and 70°, respectively. PSD functions of high-energy mode are fundamentally different from the previous mode. First, the cluster ions with E/N_{mean} = 110 eV/atom at the incident angle of 0° better smooth the surface irregularities with the spatial frequency ν above 15 μm^{-1}, but worse smooth—with ν < 15 μm^{-1}. At the incident angles of 45–70°, PSD peaks are not observed and all functions are below low-energy-functions. This corresponds to a smoother surface in whole range of spatial frequencies ν and the absence of even weakly pronounced periodic nanostructures. Thus, the nanostructures observed on AFM images (Figure 2e,f) are nonperiodic, because they have different spatial frequencies ν in accordance with the PSD-data.

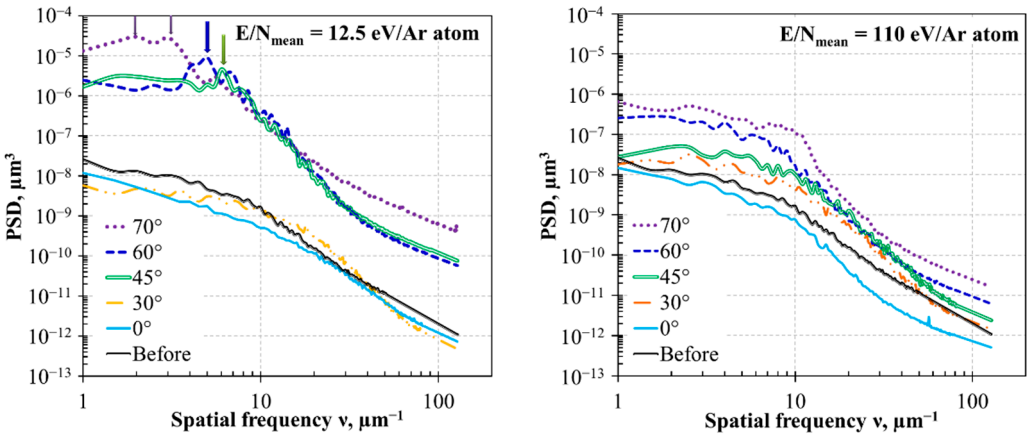

Figure 3. Power spectral density (PSD) functions of KTP surface at different incident angles of cluster ions: (**a**) after low-energy mode and (**b**) after high-energy mode.

Table 1 shows a comparison of effective roughness parameter σ_{eff} and RMS roughness parameter R_q. At both treatment modes, the surface roughness decreases to 0.28–0.30 nm at small angles (≤30°) and then significantly increases to several nanometers. It should be noted that effective roughness σ_{eff} is higher than RMS roughness R_q at low-energy mode (8–9.7%), which is most likely due to the allowance for the lateral roughness of periodic nanostructures.

Table 1. Comparison of roughness parameters.

Treatment Mode	Roughness Parameter	Before	Incident Angle of Clusters				
			0°	30°	45°	60°	70°
Low-energy mode	$\langle R_q \rangle$, nm	0.40	0.28	0.28	6.2	7.5	12.6
	$\langle \sigma_{eff} \rangle$, nm	0.43	0.28	0.30	6.8	8.1	13.8
High-energy mode	$\langle R_q \rangle$, nm	0.40	0.30	0.56	0.75	1.7	2.8
	$\langle \sigma_{eff} \rangle$, nm	0.43	0.30	0.60	0.83	1.8	2.7

4. Conclusions

The influence of fundamentally different treatment modes by the argon cluster ions on the nanostructure formation on the surface of KTP single crystals has been investigated experimentally. At normal incidence of low- and high-energy cluster ions, the surface roughness decreases to 30%. The ordered nanostructures were not observed after processing by the high-energy cluster ions (E/N_{mean} = 110 eV/atom) even at slightly higher etching depths (compared to low-energy mode) and at the small angles ($\leq 30^{\circ}$) of incidence of the cluster ions with E/N_{mean} = 12.5 eV/atom. It is assumed that the treatment by cluster ions with low energy leads to the formation of periodic nanostructures since the energy is insufficient for efficient sputtering of the target, but sufficient for a significant lateral displacement of subsurface target atoms. The most ordered nanostructures are formatted at the surface processing at angles of 45° and 60°, and they have a wavelength of 167 and 200 nm, respectively. One of the applications is the formation of periodic nanostructures on substrates of antireflective coatings to improve their quality.

Author Contributions: Conceptualization, I.V.N. and N.G.K.; methodology, N.G.K.; data acquisition, I.V.N. and N.G.K.; data processing, I.V.N.; original draft preparation, I.V.N.; review and editing, N.G.K.; visualization, I.V.N.; supervision, N.G.K. All authors have read and agreed to the published version of the manuscript.

Funding: This research was funded by the Ministry of Science and Higher Education of the Russian Federation, grant number FSUS-2020-0039.

Institutional Review Board Statement: Not applicable.

Informed Consent Statement: Not applicable.

Data Availability Statement: Data is contained within the article.

Acknowledgments: The authors acknowledge the NSU Shared Equipment Center "Applied Physics."

Conflicts of Interest: The authors declare no conflict of interest. The funders had no role in the design of the study; in the collection, analyses, or interpretation of data; in the writing of the manuscript; or in the decision to publish the results.

References

1. Sorokina, N.I.; Voronkova, V.I. Structure and properties of crystals in the potassium titanyl phosphate family: A review. *Crystallogr. Rep.* **2007**, *52*, 80–93. [CrossRef]
2. Mamrashev, A.; Nikolaev, N.; Antsygin, V.; Andreev, Y.; Lanskii, G.; Meshalkin, A. Optical Properties of KTP Crystals and Their Potential for Terahertz Generation. *Crystals* **2018**, *8*, 310. [CrossRef]
3. Pohl, K.; Bartelt, M.C.; de la Figuera, J.; Bartelt, N.C.; Hrbek, J.; Hwang, R.Q. Identifying the forces responsible for self-organization of nanostructures at crystal surfaces. *Nature* **1999**, *397*, 238–241. [CrossRef]
4. Frost, F.; Ziberi, B.; Höche, T.; Rauschenbach, B. The shape and ordering of self-organized nanostructures by ion sputtering. *Nucl. Instr. Meth. Phys. Res. B* **2004**, *216*, 9–19. [CrossRef]
5. El-Atwani, O.; Ortoleva, S.; Cimaroli, A.; Allain, J.P. Formation of silicon nanodots via ion beam sputtering of ultrathin gold thin film coatings on Si. *Nanoscale Res. Lett.* **2011**, *6*, 403. [CrossRef] [PubMed]
6. Ziberi, B.; Frost, F.; Höche, T.; Rauschenbach, B. Ion-induced self-organized dot and ripple patterns on Si surfaces. *Vacuum* **2006**, *81*, 155–159. [CrossRef]
7. Barth, J.V.; Costantini, G.; Kern, K. Engineering atomic and molecular nanostructures at surfaces. *Nature* **2005**, *437*, 671–679. [CrossRef] [PubMed]
8. Toyoda, N.; Mashita, T.; Yamada, I. Nano structure formation by gas cluster ion beam irradiation at oblique incidence. *Nucl. Instr. Meth. Phys. Res. B* **2005**, *232*, 212–216. [CrossRef]
9. Toyoda, N.; Tilakaratne, B.; Saalem, I.; Chu, W.-K. Cluster beams, nano-ripples, and bio applications. *Appl. Phys. Rev.* **2019**, *6*, 020901. [CrossRef]
10. Zeng, X.; Pelenovich, V.; Xing, B.; Rakhimov, R.; Zuo, W.; Tolstogouzov, A.; Liu, C.; Fu, D.; Xiao, X. Formation of nanoripples on ZnO flat substrates and nanorods by gas cluster ion. *Beilstein J. Nanotech.* **2020**, *11*, 383–390. [CrossRef] [PubMed]
11. Ieshkin, A.; Kireev, D.; Ozerova, K.; Senatulin, B. Surface ripple induced by gas cluster ion beam on copper surface at elevated temperatures. *Mater. Lett.* **2020**, *272*, 127829. [CrossRef]
12. Korobeishchikov, N.G.; Nikolaev, I.V.; Roenko, M.A. Effect of argon cluster ion beam on fused silica surface morphology. *Nucl. Instr. Meth. Phys. Res. B* **2019**, *438*, 1–5. [CrossRef]

13. Korobeishchikov, N.G.; Skovorodko, P.A.; Kalyada, V.V.; Shmakov, A.A.; Zarvin, A.E. Experimental and Numerical Study of High Intensity Argon Cluster Beams. *AIP Conf. Proc.* **2014**, *1628*, 885–892.
14. Korobeishchikov, N.G.; Kalyada, V.V.; Skovorodko, P.A.; Shmakov, A.A.; Khodakov, M.D.; Shulzhenko, G.I.; Voskoboynikov, R.V.; Zarvin, A.E. Features of formation of gas cluster ion beams. *Vacuum* **2015**, *119*, 256–263. [CrossRef]
15. Duparre, A.; Ferre-Borrull, J.; Gliech, S.; Notni, G.; Steinert, J.; Bennett, J.M. Surface characterization techniques for determining the root-mean-square roughness and power spectral densities of optical components. *Appl. Opt.* **2002**, *41*, 154–171. [CrossRef] [PubMed]
16. Persson, B.N.J.; Albohr, O.; Tartaglino, U.; Volokitin, A.I.; Tosatti, E. On the nature of surface roughness with application to contact mechanics, sealing, rubber friction and adhesion. *J. Phys. Condens. Matter* **2005**, *17*, R1–R62. [CrossRef] [PubMed]
17. Martínez, J.F.G.; Nieto-Carvajal, I.; Abad, J.; Colchero, J. Nanoscale measurement of the power spectral density of surface roughness: How to solve a difficult experimental challenge. *Nanoscale Res. Lett.* **2012**, *7*, 174. [CrossRef] [PubMed]
18. Bushunov, A.A.; Tarabrin, M.K.; Lazarev, V.A.; Karasik, V.E.; Korostelin, Y.V.; Frolov, M.P.; Skasyrsky, Y.K.; Kozlovsky, V.I. Fabrication of anti-reflective microstructures on chalcogenide crystals by femtosecond laser ablation. *Opt. Mat. Express* **2019**, *9*, 1689–1697. [CrossRef]